# Electronic structure of perovskite-type transition metal oxides La$MO_3$ ($M$=Ti~Cu) by U+GW approximation

Yoshiro Nohara,[1] Susumu Yamamoto,[1,2] and Takeo Fujiwara[1,2]
[1]*Center for Research and Development of Higher Education, The University of Tokyo, Tokyo 113-0033, Japan*
[2]*Core Research for Evolutional Science and Technology, Japan Science and Technology Agency (CREST-JST), Kawaguchi-shi, Saitama 332-0012, Japan*

(Received 13 December 2008; revised manuscript received 23 March 2009; published 12 May 2009)

We investigate electronic structures of La$MO_3$ ($M$=Ti~Cu) systematically by means of U+GW approximation. In these strongly correlated systems, it is important to treat large on-site Coulomb interactions and their dynamical screening effects. Transition-metal ions in perovskite-type lanthanum oxides are trivalent and their physics is qualitatively different from that of divalent transition-metal ions in transition-metal mono-oxides. The localization of wave functions of La 4$f$ and 3$d$ orbitals of Ti, V, and Co is crucial. On the other hand, the screening effect for other transition-metal 3$d$ orbitals is strong enough so as to reduce the on-site static-screened Coulomb interaction in trivalent oxides. The band gaps, the magnetic moments, and energy spectra are discussed in comparison with the experimentally observed results. Calculated energy spectra of La$MO_3$ ($M$=V~Cu) are in good agreement with experimental results.

DOI: 10.1103/PhysRevB.79.195110 PACS number(s): 71.10.−w, 71.15.−m, 71.20.Be

## I. INTRODUCTION

Strongly correlated $d$-electron systems, e.g., transition-metal oxides, show many interesting phenomena, such as a huge resistivity change caused by a small change in electron/hole concentration. Though these systems have been analyzed by the first-principles local spin-density approximation (LSDA), a full understanding is not completed. For example, the band gap, magnetic moment, and spectra are not predicted consistently with experimental values due to large on-site Coulomb interaction and the remaining of the self-interaction. On the other hand, LSDA+U method[1] with the on-site Coulomb interaction of the Hubbard-type Hamiltonian can remove the self-interaction and make wave functions localize. However, LSDA+U method is a static approach and misses the effects of dynamical screening. This problem causes several discrepancies between observed and calculated spectra.

In order to study the transition-metal oxides quantitatively, it is important to treat the correlation derived by the Coulomb interaction and dynamical screening effects. We can introduce the dynamical screening effects by means of the GW approximation (GWA),[2] which is based on the many-electron perturbation theory and treats the screening effects by the dynamical polarization. Since GWA includes the lowest terms of exchange and correlation effects in their exact forms, the self-interaction does not exist. In the case of some semiconductors or insulators, GWA opens the gap in good agreement with values experimentally observed.[3] Furthermore, since GWA calculation requires large computational resources of the CPU time and memory, the improvement and invention of algorithm are crucial.

We studied transition-metal mono-oxide systems MnO and NiO in the previous work by means of GWA and U+GWA, the GWA calculation starting from LSDA+U wave functions.[4] The GWA works quite well in antiferromagnetic MnO where the screening effect is small. On the contrary, the GWA gives rise to small on-site Coulomb interaction in NiO, since the band gap is very small and the resultant polarization function is large. Therefore, we adopted U+GWA for Ni in NiO, which deepens the 3$d$ energy level, widens the energy gap, and makes Ni$d$-O$p$ hybridization strong. The calculated spectra of MnO by GWA and NiO by U+GWA are in excellent agreement with observed ones.

Transition-metal ions in La$MO_3$ ($M$=Ti~Cu) are trivalent and qualitatively different from divalent ions in $M$O. We studied the electronic structure of antiferromagnetic $LaMnO_3$ by means of GWA.[5] The oxygen $p$ levels in the trivalent systems are shallower in energy than that in divalent systems and $M$ 3$d$ and O 2$p$ levels locate much nearer in energy. Then, the hybridization between these two levels is stronger than that in divalent systems. In other words, the $M$ 3$d$ orbitals are more delocalized and the screening effect is much stronger than in transition-metal mono-oxide systems.

In this paper, we investigate systematically, by U+GWA, the electronic structures of trivalent transition-metal oxides La$MO_3$ ($M$=Ti~Cu) and discuss the screening effects and optical spectra. The present paper is organized as follows. Section II gives a brief explanation of GWA and U+GWA. In Sec. III, we discuss the effects of the tail of the muffin-tin orbitals with the $Md$-O$p$ hybridization and the product basis. The effects of on-site Coulomb interactions $U$ of La 4$f$ and $M$ 3$d$ are discussed in Sec. IV. Summary of the effects of $U$ in $M$O and discussions on $U$ in La$MO_3$ are given here. Section V shows the results of La$MO_3$ ($M$=Ti~Cu) by U+GWA with the eigenvalue only ($e$-only) self-consistency.[6] Summary and conclusion are given in Sec. VI. In Appendix A, several trials of algorithm for calculation of realistic materials with a large unit cell are explained for saving the CPU time and memory size without a loss in accuracy. In Appendix B, the change in the off-diagonal elements of the self-energy owing to the introduction of $U$ is discussed. The discussion on the Coulomb and exchange integrals between orbitals is given in Appendix C.

 

## II. BRIEF NOTE FOR GW APPROXIMATION

### A. GW approximation

GWA is the first-term approximation of Hedin's equation[2] and, for realistic materials, formulated usually with the LSDA Hamiltonian as an unperturbed one. The GWA self-energy is written as

$$\Sigma = iG_0W, \tag{1}$$

where $G_0$ is the unperturbed Green's function. $W$ is the dynamically screened Coulomb interaction which is usually calculated with the random-phase approximation and is written as

$$W = v + v\chi^0 W = v + W_C, \tag{2}$$

where $v$ is the bare Coulomb interaction and $\chi^0$ is the lowest-order irreducible polarization function $\chi^0 = -iG_0G_0$. Correspondingly, the self-energy can be divided in two parts; the contribution from the exchange interaction $\Sigma_X = iG_0v$ and that of the correlation $\Sigma_C = iG_0W_C$.

GWA does not include the vertex correction and ladder diagrams (corresponding to processes of electron-electron, electron-hole, and hole-hole scatterings), which cause nonvanishing imaginary part of the self-energy near the band gap in the spectrum of insulators.[7]

### B. U+GWA: GWA starting from LSDA+U

Standard GWA is carried out with no self-consistent procedure and calculated results depend strongly on the starting wave functions. We proposed an alternative method of GWA with wave functions obtained by LDA+U, named U+GWA,[4] with the $e$-only self-consistency. LSDA+U method can produce localization of wave functions, and wave functions and eigenvalues are improved much in this procedure. LSDA+U method is a kind of static limit of GWA (Ref. 8) and it is natural to start GWA from LSDA+U if we want to start with wave functions localized more than those of LSDA. Once opening a band gap, the resultant polarization function is reduced and the screening effect becomes weaker.

Since we start with the LSDA+U Hamiltonian $H_{\mathrm{LSDA+U}}$, the exchange-correlation potential $V^{\mathrm{XC}}_{\mathrm{LSDA}}$ and the potential correction $V^{\mathrm{corr}}_{\mathrm{LSDA+U}}$ derived from the Hubbard term should be subtracted from the GWA self-energy Eq. (1) as

$$\Delta\Sigma = iG_0W - V^{\mathrm{XC}}_{\mathrm{LSDA}} - V^{\mathrm{corr}}_{\mathrm{LSDA+U}}, \tag{3}$$

and Green's function $G$ is defined as

$$G(E) = [E - H_{\mathrm{LSDA+U}} - \Delta\Sigma(E)]^{-1}. \tag{4}$$

The quasiparticle energy $E_{\mathbf{k}n}$ should be calculated as

$$E_{\mathbf{k}n} = \epsilon_{\mathbf{k}n} + \mathrm{Re}\ \Delta\Sigma_{\mathbf{k}n}(E_{\mathbf{k}n}), \tag{5}$$

where $\epsilon_{\mathbf{k}n}$ is the LSDA+U eigenenergy.

In our preceding work,[4] we demonstrated that the value of $U$ should be chosen in U+GWA so that the energy difference between two principal peaks in the occupied and unoccupied bands is equal to the that in observed spectra. The screened static Coulomb interaction $W(0)$ is the outcome in U+GWA.

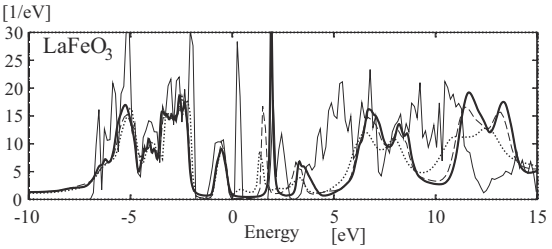


FIG. 1. Convergence behavior of the spectrum (the imaginary part of the total Green's function $\frac{1}{\pi}|\mathrm{Im}\ G(\omega)|$) of $LaFeO_3$ by the $e$-only self-consistent calculation. The calculation is based on U+GWA and $U$ and $J$ values for La $4f$ orbital are 7.5 and 0.5 eV, respectively. LSDA+U: thin solid line, U+GWA (first iteration): dotted line, U+GWA (second iteration step): thin broken line, U+GWA (third iteration step): bold solid line. The energy zeroth is fixed at the Fermi energy $E_F$ of respective iteration step.

### C. Eigenvalue-only self-consistency

GWA calculation is carried out conventionally without self-consistent procedure and then, the results depend strongly on the starting wave functions. Surh *et al.*[6] proposed the eigenvalue only ($e$-only) self-consistent procedure updating eigenvalues but not wave functions. Throughout the present work, we carry out the $e$-only self-consistent calculation.

Figure 1 shows the spectrum of $LaFeO_3$ at each iteration step of the $e$-only self-consistent procedure. At the third iteration step, the spectral change is negligible. The final shape of spectra becomes sharper and the band gap clearer.

## III. TAIL OF MUFFIN-TIN ORBITALS AND IMPROVEMENT OF PRODUCT BASIS

Calculation in the present work is based on the tight-binding linear muffin-tin orbital (LMTO) method with the atomic sphere approximation,[9] and basis wave functions are muffin-tin orbitals (MTO) centered at their respective atom positions. Then, the costs of GWA is proportional to $n^6$, where $n$ is the number of the MTO basis in a unit cell. In order to reduce the costs, the product basis scheme[10] is employed in the calculation of the polarization and the self-energy.

Products of wave functions, $\psi^*_{k'}\psi_{k'+q}$ or $\psi^*_k\psi_{k-q}$, appear at the vertices of the Coulomb interaction $v$ and its screened interaction $W$ in Fig. 2. When one uses this product of wave functions as a one function, the calculation cost is written as $O(n^2 \times n_p^2)$, where $n_p$ is the number of the product basis. Then, if the number of the products is reduced, the calculation cost can be reduced much. The product basis functions can be classified according to their total angular momentum and those with larger total angular momentum can be eliminated in $\Sigma_C$ without any additional error.[11,12] We call this procedure "the angular momentum elimination." The "angular momentum elimination" could not be done in the calculation of $\Sigma_X$ because of non-negligible error.

The radial parts of the product of wave functions are the product of $\phi\phi$, $\phi\dot{\phi}$, and $\dot{\phi}\dot{\phi}$, where $\phi$ is a radial wave func-

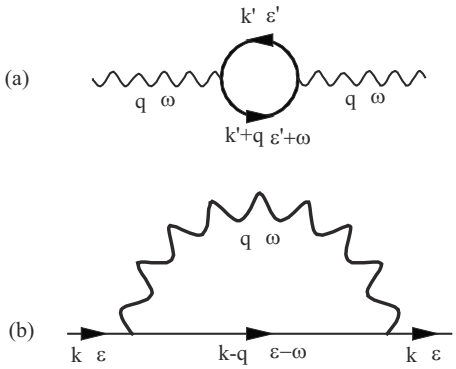


FIG. 2. Feynman diagrams of the basic contributions to GWA; (a) the polarization and (b) the exchange self-energy. The products of wave functions, $\psi^*_{k'}\psi_{k'+q}$ or $\psi^*_k\psi_{k-q}$, appear at each vertex.

tion of LMTO defined within atomic spheres and $\dot{\phi}$ is its energy derivative.[9] In our earlier works,[5,11,12] we adopted radial wave functions of only $\phi\phi$ but not $\phi\dot{\phi}$ and $\dot{\phi}\dot{\phi}$. However, the oxides with trivalent transition-metal ions are expected to have a large amount of hybridization mixing between $M$ $3d$ and O $2p$ orbitals. The $\dot{\phi}$ within a $M$ atomic sphere is the contribution of the tail of wave functions of nearest-neighbor O and becomes more important in oxide systems. In other words, $\dot{\phi}$ plays much important role in the hybridization mixing between two orbitals with different energy centers ($E_v$). The contribution from $\phi\dot{\phi}$ and $\dot{\phi}\dot{\phi}$ was then included in our recent work.[4]

The product basis functions $\{\phi\phi$, $\phi\dot{\phi}$, and $\dot{\phi}\dot{\phi}\}$ are not orthogonal with each other and had better be expanded in terms of orthogonalized functions. When we use only $\phi\phi$-type product basis functions, the diagonalization procedure can be achieved by means of the Cholesky decomposition (LU decomposition) and we can use the resultant orthogonal basis functions efficiently. However, this method does not work well when we include $\phi\dot{\phi}$-type and $\dot{\phi}\dot{\phi}$-type basis functions, because the product basis functions may be over complete and the product matrix is almost singular. Moreover, a serious practical problem is that the total number of product basis is huge. Therefore, we orthonormalize the product basis by the Gram-Schmidt orthonormalization method. In the Gram-Schmidt procedure, the original product basis are reordered according to the number of nodes, and the product basis with a fewer nodes are preferentially accepted. In this way, we can discard the last half of those basis with more nodes and this process is called the "radial-node elimination." As a result, the total number of the product basis can be reduced by 50% without an additional error both in $\Sigma_C$ and $\Sigma_X$.

Actual procedure of elimination of product basis is as follows: First, "the radial-node elimination" procedure reduces the number of product basis functions by 50% both in $\Sigma_C$ and $\Sigma_X$. Next, "the angular momentum elimination" procedure reduces the number of the basis functions by 10%, 30%, and 50% in the total angular momentum $l=0$, 1, and 2, respectively, of $\Sigma_C$. As a result, the total number of the product basis is reduced in $\Sigma_C$ by 50% ($l=0$), 60% ($l=1$), 80% ($l=2$), and 100% ($l\geq 3$) and in $\Sigma_X$ by 50% for all total angular momentums. This effort of including $\phi\dot{\phi}$ and $\dot{\phi}\dot{\phi}$ improves the accuracy much with keeping the computational costs as before.

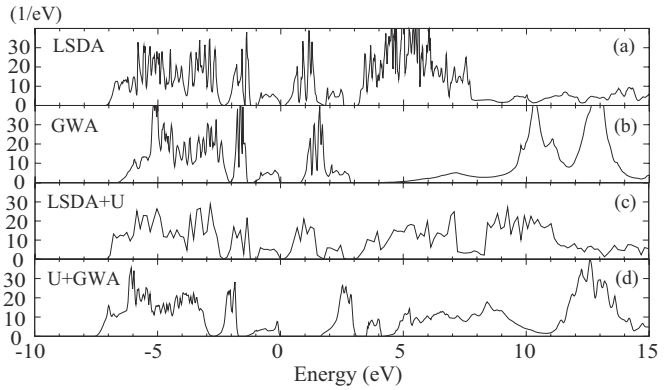


FIG. 3. Quasiparticle density of states of $LaMnO_3$. (a) LSDA, (b) GWA quasiparticle (QP) (Ref. 5), (c) LSDA+U, and (d) U+GWA QP. (c) and (d) are the results of the present work with the parameters of $U=7.5$ eV and $J=0.5$ eV for La $4f$.

## IV. $U$ VALUES FOR U+GWA

### A. Effect of $U$ of La $4f$ orbitals

In the LSDA, the unoccupied bands in the energy range of 5 eV above $E_F$ are mainly of La $4f$ and $5d$ character and these bands overlap with strong hybridization. The levels of La $4f$ locate too low in energy and the occupation is, for example in $LaMnO_3$, 0.32 per spin. Then the GWA lifts the $4f$ components up to higher energies at about 10 eV above $E_F$ and the $5d$ components move together due to strong hybridization.[5] This result disagrees with experimental observation. If La $4f$ levels can be lifted up in a starting calculation, La $5d$ bands may stay in an appropriate energy region.

In the present work, we adopt the LSDA+U method for La $4f$ levels as the unperturbed Hamiltonian, values of $U=7.5$ and $J=0.5$ eV of La $4f$ are used in LSDA+U, evaluated by the "constrained LSDA" (c-LSDA).[13] $U$ value of the c-LSDA is usually too large since c-LSDA kills some screening channels on target orbitals. In the present case, La $4f$ levels are much higher in energy than $E_F$ and do not affect main screening effects caused by occupied $M$ $3d$ states. On the contrary, it is not necessary to introduce $U$ value for La $5d$ levels in the unperturbed Hamiltonian, because La $5d$ electrons feel that the weak atomic potential screened by inner La $3d$ and $4d$ electrons and the wave functions are extended well.

Figure 3 shows the results with and without $U$ of La $4f$. GWA starting from LSDA eigenvalues and wave functions gives rise to large energy shifts for hybridized La $4f$ and $5d$ states. LSDA+U calculation splits the La $4f$ and $5d$ bands and then the U+GWA makes La $4f$ and $5d$ bands appear separately at around 12.5 and 7 eV above $E_F$, respectively, consistently with observed spectra as shown in Fig. 4.

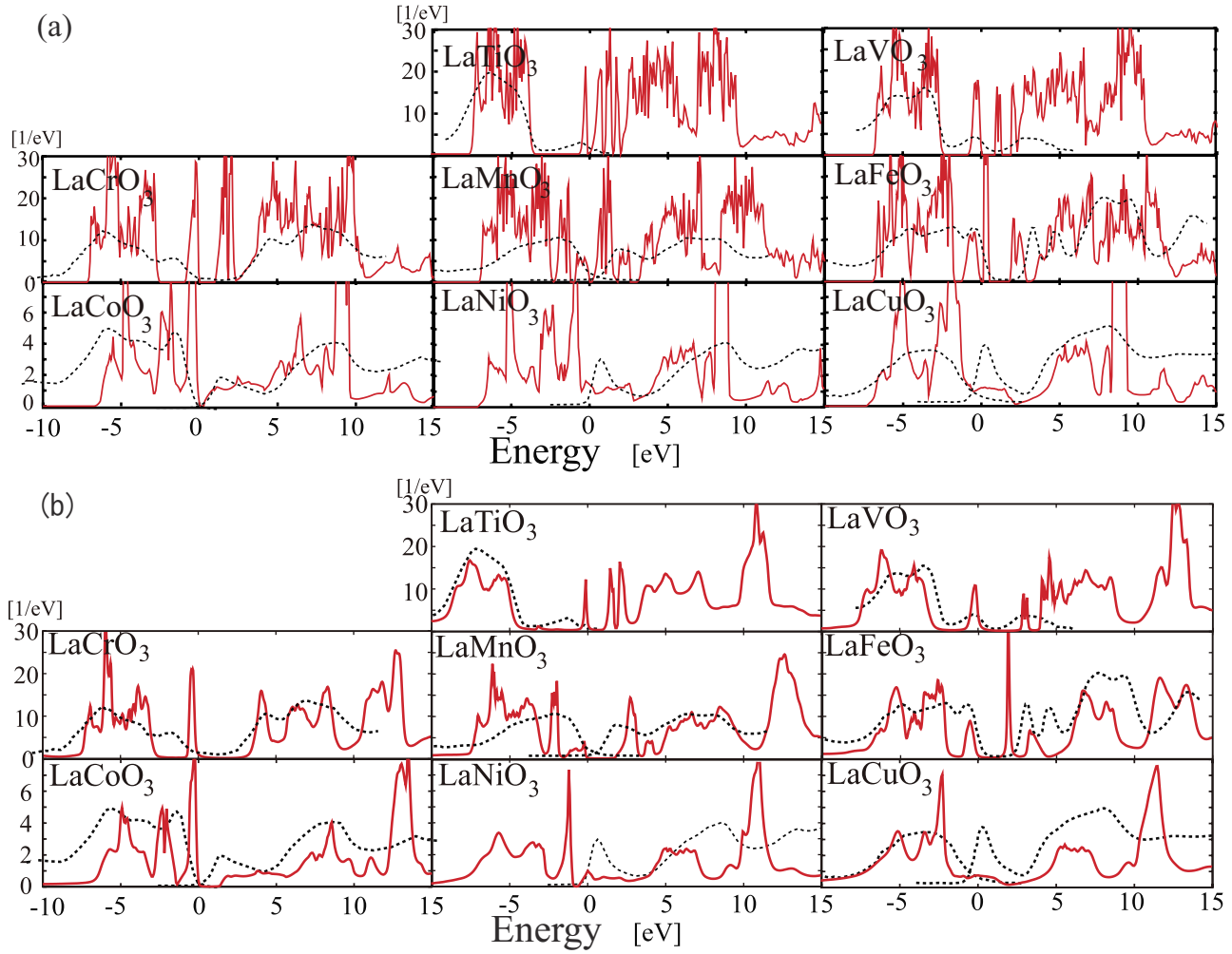


FIG. 4. (Color online) Imaginary part of Green's functions $(1/\pi)|\mathrm{Im}\, G(\omega)|$ (per unit cell) of La$M$O$_3$ ($M$=V~Cu) where the energy zeroth is set at the Fermi energy $E_F$. (a) those by LSDA+U (starting spectra), and (b) those by U+GWA at third iteration. In all cases, La $4f$ orbitals are treated by LSDA+U/U+GWA with $U$=7.5 eV and $J$=0.5 eV. For transition-metal ions, $U$ and $J$ are used for Ti ($U$=2.5 eV, $J$=1.0 eV), V ($U$=3.0 eV, $J$=1.0 eV) and Co ($U$=2.7 eV, $J$=1.3 eV). It should be noted that the unit cells of La$M$O$_3$ ($M$=Ti,V,Cr,Mn,Fe) contain four molecular units and those of $M$=Co,Ni,Cu contain one unit. The dotted lines in (a) and (b) are the experimental spectra and are shown in arbitrary intensity scale. The original experimental data can be found in the following references: LaTiO$_3$ (Ref. 48), LaVO$_3$ (Ref. 49), LaCrO$_3$ (Ref. 50), LaMnO$_3$ (Ref. 35), LaFeO$_3$ (Ref. 38), LaCoO$_3$ (Ref. 39), LaNiO$_3$ (Ref. 40), and LaCuO$_3$ (Ref. 41).

### B. Effect of $U$ of trivalent transition-metal $d$ orbitals

#### 1. Divalent transition-metal ions in MO

In our recent work proposing the novel U+GWA,[4] the electronic energy spectra were calculated in divalent transition-metal ion systems, NiO and MnO. In these systems, $O^{2-}$ $2p$ and $M^{2+}$ $3d$ levels are energetically separated widely.

Antiferromagnetic MnO is a system of localized $3d$ bands with fully spin-polarized $(t_{2g}^{\uparrow})^3(e_g^{\uparrow})^2$ configuration and a small screening effect does work because of small polarization of $M^{2+}$ $d \rightarrow d$ transition. This gives rise to the large static-screened Coulomb interaction $W(0)$ by GWA, which is consistent with the observation.

The electron configuration of $Ni^{2+}$ in NiO is $(t_{2g}^{\uparrow})^3(t_{2g}^{\downarrow})^3(e_g^{\uparrow})^2$ and the polarization function is large due to the $d(t_{2g}^{\downarrow}) \rightarrow d(e_g^{\downarrow})$ transition. In addition to this, because of the narrow LSDA energy gap, the screened Coulomb interaction $W(0)$ becomes small in GWA. However, real positions of the oxygen $p$ levels should be at energies slightly nearer to the top of the occupied bands. Therefore, we adopted U+GWA for NiO where the finite $U$ value makes the starting nickel $d$ level deeper (resultantly, oxygen $p$ levels shallower) due to the self-interaction correction and the energy gap wider. The finite $U$ value of $Ni^{2+}$ is determined so as to obtain good agreement of the energy separation between principal peaks in calculated and experimental XPS-BIS spectra.

#### 2. Trivalent transition-metal ions in LaMO$_3$

Perovskite-type transition-metal oxides are systems of trivalent transition-metal ions and the situation is qualitatively different from cases of divalent transition-metal mono-

TABLE I. Spin and orbital orders, metal or insulator, lattice symmetry, and structure of perovskite $3d$ transition-metal oxides La$M$O$_3$, $M$=Ti~Cu. In "Spin order" column, AFM, NM, and PM denote "antiferromagnetic," "nonmagnetic," and "paramagnetic," respectively. Also in 'Symmetry' column, $O$, $M$, $R$, and $T$ denote "orthorhombic," "monoclinic," "rhombohedral," and "tetragonal," respectively. The spin and orbital order types, $A$, $C$, and $G$, should be referred to Ref. 14.

| | Ti | V | Cr | Mn | Fe | Co | Ni | Cu |
|---|---|---|---|---|---|---|---|---|
| Spin order | $G$-AFM[15] | $C$-AFM[16,17] | $G$-AFM[18] | $A$-AFM[19] | $G$-AFM[18] | NM*[a] | PM[21] | PM |
| Orbital order | **[b] | $G$[c] | | ***[d] | | | | |
| Metal(M) or Insulator(I) | I | I | I | I | I | I | $M$ | $M$ |
| Symmetry | $O$ | $M$ | $O$ | $O$ | $O$ | $R$ | $R$ | $T$ |
| Structure | Ref. 22 | Ref. 29 | Ref. 30 | Ref. 19 | Ref. 31 | Ref. 18 | Ref. 18 | Ref. 32 |

[a]LaCoO$_3$ is nonmagnetic at the low temperatures and the $Co^{3+}$ ion is in the low-spin ($t_{2g}^6$:$^1A_1$) configuration. The system seems to change to the intermediate spin state ($t_{2g}^5e_g$:$^3T_1$) at around 90 K (Ref. 20).
[b]Sizable deformation and the orbital order are observed in Ref. 22. For detail discussion on orbital order, see the text.
[c]Stabilization of coexistence of $C$-AFM and $G$-type orbital order is discussed in Ref. 23
[d]Refs. 24 and 25. There are several reports of experimental observation. $C$-type antiferromagnetic orbital order by the resonant x-ray scattering (Ref. 26). Recent ESR (Ref. 27) and neutron diffraction (Ref. 28) experiments report different orbital order. Detail discussion will be given in Sec. V D 4.

oxides. In most cases ($M$=Cr~Cu), the atomic potential of oxygen $p$ electrons becomes shallow and the separation between $O^{2-}$ $2p$ and $M^{3+}$ $3d$ levels becomes much smaller. Then, $O^{2-}$ $2p$ states are well hybridized with $M^{2+}$ $d$ states in the top of the valence bands. Moreover, GdFeO$_3$-type distortion of $MO_6$ octahedra causes the $t_{2g}$-$e_g$ mixing in $M^{3+}$ ions in $M$=Ti~Fe. Therefore, the $d$-$d$ screening is quantitatively large in the perovskite-type structure. We categorize trivalent transition-metal ions $M^{3+}$ into two, one of which may have strong screening effects and the other is the rest.

Most trivalent transition-metal ions, $Cr^{3+}$, $Mn^{3+}$, $Fe^{3+}$, $Ni^{3+}$, and $Cu^{3+}$, belong to the first category. In $Cr^{3+}$, $Mn^{3+}$, and $Fe^{3+}$ systems, transition-metal ions are well spin polarized and $O^{2-}$ $2p$ levels locate near $3d$ levels in LSDA. As a result, these systems are affected by large screening effects due to the extended $d$ orbitals over $O^{2-}$ $2p$ orbitals and small-screened on-site Coulomb interaction. In the cases of $M^{3+}$=$Ni^{3+}$ and $Cu^{3+}$, the systems are paramagnetic metals without the GdFeO$_3$-type distortion and $d$-orbital wave functions of $M^{3+}$ ions hybridize strongly with $O^{2-}$ $p$ orbitals. Therefore, they are affected by strong screening effects too. For the first category, it is not necessary to introduce $U$ in $M^{3+}$ because of the resultant strong screening effect and this effect is reproduced satisfactory without $U$ (in U+GWA calculations).

Light ions, $M^{3+}$=$Ti^{3+}$ and $V^{3+}$, are of the second category. For these two cases, $O^{2-}$ $p$ levels locate deeper in energy. A calculation with $U$=0 in $M^{3+}$ gives rise to a partially filled $t_{2g}^{\uparrow}$ bands with large polarization function. This situation causes a large screening effect and the resultant ground state is metallic in both materials. The correct situation may be the partially filled $t_{2g}^{\uparrow}$ bands but a larger (screened) Coulomb interaction creates an appropriate band gap. To have a good starting state in $Ti^{3+}$ and $V^{3+}$ or, in other words, to keep appropriate $d$-energy positions, we need to introduce a finite value of $U$ and keep an energy gap finite.

$Co^{3+}$ may be an exception. LaCoO$_3$ is a nonmagnetic insulator but calculated result is metallic, if we would not use a finite $U$ in $Co^{3+}$ ion. Therefore, we should start with a finite $U$ value to keep the band gap finite. This case will be discussed more in Sec. V D.

## V. RESULTS AND DISCUSSIONS

### A. Calculation detail

The perovskite-type transition-metal oxides show a large variety of spin and orbital order and lattice distortion. The crystal structure and the spin and orbital orderings are summarized in Table I. They are the $G$, $C$, $G$, $A$, and $G$-type antiferromagnetic spin-ordered insulators at low temperatures as $M$ changes from Ti to Fe. (For the order types, $A$, $C$ and $G$, one can refer to Ref. 14.) La$M$O$_3$ is nonmagnetic insulator for $M$=Co and paramagnetic metal for $M$=Ni and Cu. The orbital order is found in LaTiO$_3$, LaVO$_3$, and LaMnO$_3$ at low temperatures and presumably in LaCoO$_3$ at intermediate temperature range. The crystal lattices are orthorhombic for $M$=Ti, Cr, Mn, and Fe, monoclinic for $M$=V, rhombohedral for LaCoO$_3$ and LaNiO$_3$ and tetragonal for LaCuO$_3$. The unit cell contains four molecular units of La$M$O$_3$ in $M$=Ti, V, Cr, Mn, Fe, and one unit in $M$=Co,Ni,Cu.

We adopt $4\times4\times4$ **k** mesh points in Brillouin zone for $M$=Ti~Co and $8\times8\times8$ **k** points for $M$=Ni~Cu. The calculation is based on the tight-binding linear muffin-tin orbital (LMTO) method and we use empty spheres of 20 (Ti, V), 16 (Cr~Fe), and 12 (Co~Cu), and totally 17–40 atomic spheres exist in a unit cell. The set of the maximum orbital angular momentum of the LMTO basis in La, $M$, and O empty spheres are chosen to be ($fddp$). In the calculation of the self-energy, the maximum total angular momentums of the product basis is set to be ($fddp$) for the calculation of the correlation part of the self-energy $\Sigma_C$ and ($iffd$) for $\Sigma_X$. This choice and "the radial-node elimination" reduce the number of the product basis used in $\Sigma_C$ from 4428 to 756 for the case of $M$=Ti and V, from 4296 to 720 for $M$=Cr~Fe, and from

TABLE II. The Coulomb and exchange interactions $U$ and $J$, magnetic moment $M$ of the transition-metal $3d$ orbitals, the direct gap $E_{G:d}$, and the indirect gap $E_{G:id}$ by LSDA+U and U+GWA, compared with the experimental ones, the occupations (per one atom) of $d$-orbital electrons with majority (↑) /minority (↓) spin $n_{d\uparrow/\downarrow}$, and total $d$ occupation $n_d$, the high and low-frequency limit of screened Coulomb interactions $W(\infty)$ and $W(0)$, and the ratio of them $W(0)/W(\infty)$. If finite values of $U$ and $J$ are given in "LSDA+U" column, the LSDA+U/U+GWA calculations are carried out with these $U$ and $J$ values for $M$ $d$ orbitals, otherwise, zero values of $U$ and $J$ are used for $M$ $d$ orbitals. In all cases, $U=7.5$ and $J=0.5$ eV are used for La $4f$ orbitals in LSDA+U/U+GWA calculations. The band gaps are evaluated from the structure of the quasiparticle bands.

| | | Ti | V | Cr | Mn | Fe | Co | Ni | Cu |
|---|---|---|---|---|---|---|---|---|---|
| Constraint LSDA | $U$(eV) | 8.2 | 7.6 | 7.8 | 8.0 | 8.3 | 7.8 | 8.1 | 8.5 |
| | $J$(eV) | 0.90 | 0.84 | 0.84 | 0.90 | 0.87 | 0.84 | 0.87 | 0.93 |
| Experimental | $U$(eV) [a] | 4.0[34] | 4.0[36] | 5.2[34] | 7.8,[35]7.5[37] | 7.5,[37]6.0[38] | 5.5[39] | 7[40] | 7.0[41] |
| Spectra | $J$(eV) [b] | 1.0 | 1.0 | 1.1 | 1.1 | 1.2 | 1.3 | 1.3 | |
| | $M(\mu_B)$ | 0.45[15] | 1.3[16] | 2.45,2.8[18,43] | 3.87[19] | 3.9,4.6[18,44] | | | |
| | $E_{G:d}$(eV) | 0.1[45] | 1.1[45] | 3.4[45] | 1.1[45] | 2.1[45] | 0.3[45] | 0[45] | 0[45] |
| LSDA+U | $U$(eV) | 2.5 | 3.0 | | | | 2.7 | | |
| | $J$(eV) | 1.0 | 1.0 | | | | 1.3 | | |
| | $n_{d\uparrow}$ | 1.38 | 2.48 | 3.39 | 4.29 | 4.85 | 3.60 | 4.11 | 4.60 |
| | $n_{d\downarrow}$ | 0.70 | 0.71 | 0.85 | 0.83 | 1.31 | 3.60 | 4.11 | 4.60 |
| | $n_d$ | 2.08 | 3.19 | 4.24 | 5.12 | 6.16 | 7.21 | 8.22 | 9.21 |
| | $W(\infty)$(eV) | 20.12 | 21.18 | 22.39 | 23.86 | 24.85 | 27.73 | 29.04 | 29.31 |
| | $W(0)$(eV) | 2.25 | 3.49 | 3.01 | 2.54 | 1.86 | 3.96 | 1.12 | 1.69 |
| | $W(0)/W(\infty)$ | 0.11 | 0.16 | 0.13 | 0.11 | 0.07 | 0.14 | 0.04 | 0.06 |
| | $M(\mu_B)$ | 0.68 | 1.79 | 2.58 | 3.50 | 3.54 | | | |
| | $E_{G.d}$(eV) | 0.49 | 0.92 | 1.04 | 0.46 | 0.10 | 0.49 | | |
| | $E_{G.id}$(eV) | 0.01 | 0.86 | 1.02 | 0.11 | 0.10 | 0.23 | | |
| U+GWA | $W(0)$(eV) | 3.09 | 4.73 | 4.28 | 3.82 | 3.03 | 4.72 | 1.00 | 1.59 |
| | $W(0)/W(\infty)$(eV) | 0.15 | 0.22 | 0.19 | 0.16 | 0.12 | 0.14 | 0.03 | 0.05 |
| | $M(\mu_B)$ | 0.68 | 1.79 | 2.38 | 3.16 | 3.37 | | | |
| | $E_{G:d}$(eV) | 1.00 | 2.48 | 3.28 | 1.79 | 1.78 | 1.68 | | |
| | $E_{G:id}$(eV) | 0.77 | 2.47 | 3.25 | 1.63 | 1.76 | 1.28 | | |

[a] $U$ determined from cluster-CI calculations so as to have good agreement with observed results by x-ray photoemission spectroscopy (XPS) and x-ray absorption spectroscopy (XAS).

[b] Calculated from the Slater integrals $F^2$ and $F^4$ in Ref. 42.

1338 to 252 for $M=$Co$\sim$Cu per spin. In the calculation of the exchange part of the self-energy $\Sigma_X$, we reduce the number of the product basis from 9096 to 4724 for $M=$Ti and V, from 8964 to 4648 for $M=$Cr$\sim$Fe, and from 2505 to 1314 for $M=$Co$\sim$Cu per spin.

We calculate the electronic structures by U+GWA with the $e$-only self-consistency. For all systems, at the third iteration step of the $e$-only self-consistent calculation, the energy shift becomes very small and the whole calculation almost converges.

### B. Screened on-site Coulomb interaction of transition-metal ions

Values of $U$ and $J$ for transition-metal ions used in the LSDA+U and U+GWA calculations are listed in the "LSDA+U" column of Table II, together with the estimated values of static-screened on-site Coulomb interaction $W(0)$ of transition-metal $3d$ orbitals. If we use, in U+GWA calculation, $U$ values evaluated by c-LSDA, we would obtain a wider energy separation between principal peaks of occupied and unoccupied bands and a wider band gap. Furthermore, the resultant $W(0)$ values become too large. In fact, we need not introduce $U$ for $3d$ orbitals of most transition-metal ions.

The calculated values of the screened Coulomb interaction $W(0)$ for $Ti^{3+}\sim Cr^{3+}$ are similar to the $U$ values by the cluster-CI calculation. The resultant band gaps of $Cr^{3+}$, $Mn^{3+}$, and $Fe^{3+}$ are comparable with the observed ones. The calculated $W(0)$ in $Mn^{3+}$ is much smaller than the $U$ values of the cluster-CI calculation, but shows a good agreement with an experimentally determined one.[33] For Co, we need to introduce a finite $U$. The resultant energy gap may be too large and $W(0)$ is comparable with that in the cluster-CI calculation. In the cases of Ni and Cu, the values of $W(0)$ are small because of the metallic screening.

The static-screened Coulomb interactions $W(0)$ evaluated here are different from both those of cluster-CI models and those of the c-LSDA. It should be stressed that the calculated $W(0)$ are comparatively small. This may not be a surprising result, once we compare the O $2p$-$M$ $3d$ separation in $M^{3+}$ and $M^{2+}$ systems. Furthermore, our $W(0)$ includes effects of screening by $d$ electrons but $U$ in cluster-CI models does not.

TABLE III. The $d \rightarrow d$ unscreened Coulomb interaction $W_r(0)$ (eV) of $LaFeO_3$ by U+GWA. The energy window is set between $E_{min}$ (eV) and $E_{max}$(eV) The fully screened Coulomb interaction is $W(0)=3.03$ eV. The energy zeroth is at the top of the valence bands.

| $W_r(0)$ | $E_{min}$ | $E_{max}$ |
|---|---|---|
| 5.36 | −1.36 | 4.63 |
| 9.28 | −4.63 | 4.63 |

It should be noted that the result by c-LSDA is that with switching some screening channels off. To compare $W(0)$ with $U$ in c-LSDA, we should see the effects of switching off in the polarization function. The Coulomb interaction $W_r$, which does not include the $d \rightarrow d$ polarization, is evaluated by means of the following equation;[46]

$$W_r(E) = [1 - vP_r(E)]^{-1}v, \tag{6}$$

where $P_r$ is the polarization function excluding the $d \rightarrow d$ transition process and $v$ is the bare Coulomb interaction matrix. It is difficult to distinguish whether a specified band is of the $d$ character or not in an actual calculation of such complex systems and, moreover, if we project out the $d$ components of each band, a real part of $W_r(E)$ sometimes becomes negative. In our present work, we define the "$d$ bands" with a help of an energy window, and, if the initial and final states locate in this energy window, we exclude this process in the calculation of the polarization function $P_r$. Table III shows the calculated values of the Coulomb interaction $W_r(0)$ with respective energy windows which we exclude the calculation as $d \rightarrow d$ transition. The values of $W_r(0)$ are comparable to $U$ of c-LSDA.

We can estimate the values of $W(0)$ from the energy separation between principal peaks in occupied and unoccupied bands corresponding to the particular electron configuration. Then we will show, in Sec. V D, the consistency between the calculated values of $W(0)$ in the calculated optical spectra. In other words, the main profile of the optical spectra is determined by $W(0)$.

### C. Spin magnetic moments

The calculated values of the magnetic moment are listed in Table II and compared with the observed ones.[15,16,18,19,43,44] The data show good agreement with experiments. Since the calculation of U+GWA is based on the $e$-only self-consistency, the resultant magnetic moment is essentially the same as that by LSDA+U.

### D. Optical spectra

The direct and indirect band gaps ($E_{G:d}$ and $E_{G:id}$) of $LaMO_3$ ($M$=Ti~Cu) are summarized in Table II, evaluated from the calculated quasiparticle bands. The band gap would be smeared out and become narrower if we could include the contribution by ladder diagrams (i.e., the electron-electron, electron-hole, and hole-hole scatterings) in the higher approximation.[7,47] The observed $O^{2-}$ $p$ bands move to higher energy side with changing transition-metal ions from $Ti^{3+}$ to $Cu^{3+}$. This fact is consistent with the observed crossover of the band gap from the Mott-Hubbard gap in $M$=Ti and V to the charge-transfer (CT) gap in $M$=Cr~Cu.[45]

The calculation starts from the LSDA+U results shown in Fig. 4(a) and the U+GWA spectra are shown in Fig. 4(b) with experimentally observed results of x-ray photoemission spectroscopy (XPS) and x-ray absorption spectroscopy (XAS).[35,38–41,48–50] The projected spectra of U+GWA are also shown in Fig. 5 by using the local coordinate system where the $z$ axis is along the direction of the $M$-O pair of the longest interatomic distance and other $x$ and $y$ axes direct to the directions of other $M$-O pairs.

#### 1. $LaTiO_3$

The ground state of $LaTiO_3$ is an antiferromagnetic insulator. The electron configuration of $Ti^{3+}$ is $(t_{2g}^{\uparrow})^1$. The LSDA+U method cannot make the system insulating if one would use smaller values of $U \leq 2.3$ eV. The starting LSDA+U state is an antiferromagnetic insulator of a narrow indirect gap of 0.01 eV with $U=2.5$ eV [Fig. 4(a)]. Both the top of the occupied band and the bottom of unoccupied band are of the majority spin. The bands are broadened in U+GWA, owing to the shift of the Ti and La $d$ states, La $f$ states, and hybridization between Ti $d$ and O $p$ states.

The top of occupied oxygen $2p$ band locates at 4.5 eV below the occupied Ti $d_{(yz-zx)/\sqrt{2}}$ orbital in the calculated spectra (Fig. 5) which is in good agreement with observation. The energy separation between two principal peaks of occupied $t_{yz-xz}^{\uparrow}$ and unoccupied $t_{yz+xz,xy}^{\uparrow}$ bands in U+GWA (−0.2 and 1.5 eV) is about 1.7 eV, and this may be estimated as

$$\{E_T[(t_{2g}^{\uparrow})^2] - E_T[(t_{2g}^{\uparrow})^1]\} - \{E_T[(t_{2g}^{\uparrow})^1] - E_T[(t_{2g}^{\uparrow})^0]\} = u'_{t_{2g}} - j_{t_{2g}} = U - 1.17J, \tag{7}$$

where $E_T(\Gamma)$ is the total energy of the multiplet $\Gamma$, $u'_{t_{2g}}$ and $j_{t_{2g}}$ are the Coulomb and exchange integrals between $t_{2g}\xi$ and $t_{2g}\eta$ orbitals (see Appendix C) Once we replace $U$ in Eq. (7) by $W(0)$ and $J$ by the used one in U+GWA, the calculated result, $W(0)=3.09$ eV, is consistent with the above separation 1.7 eV.

The indirect and direct gaps are 0.77 and 1.0 eV, respectively, in U+GWA as shown in Table II. This finite band gap might be an artifact due to our unavoidably larger value of $U=2.5$ eV for the starting insulating state. Arima *et al.*[45] reported the optical conductivity data that the Hubbard band gap is 0.1 eV and the CT gap (the transition from O $2p$ to Ti $3d$) is 4.5 eV.

The local distortion of octahedron elongation splits the degeneracy of $d_{xz}$ and $d_{yz}$ of titanium into $d_{(yz-zx)/\sqrt{2}}$ and $d_{(yz+zx)/\sqrt{2}}$. According to the diagonalization of the density matrix of one particular titanium ion, the main part of $3d$ states of this titanium ion is approximately $(-0.30|xy\rangle + 0.96|(yz-xz)/\sqrt{2}\rangle)$. The main part of $3d$ states in the eigenvector at the top of the highest occupied band ($\Gamma$ point) is approximately $(-0.468|xy\rangle + 0.884|(yz-zx)/\sqrt{2}\rangle)$, which is in good agreement with the analysis by Cwik *et al.*[22] 64% of the weight at $\Gamma$ point is on titanium ions. The rest compo-

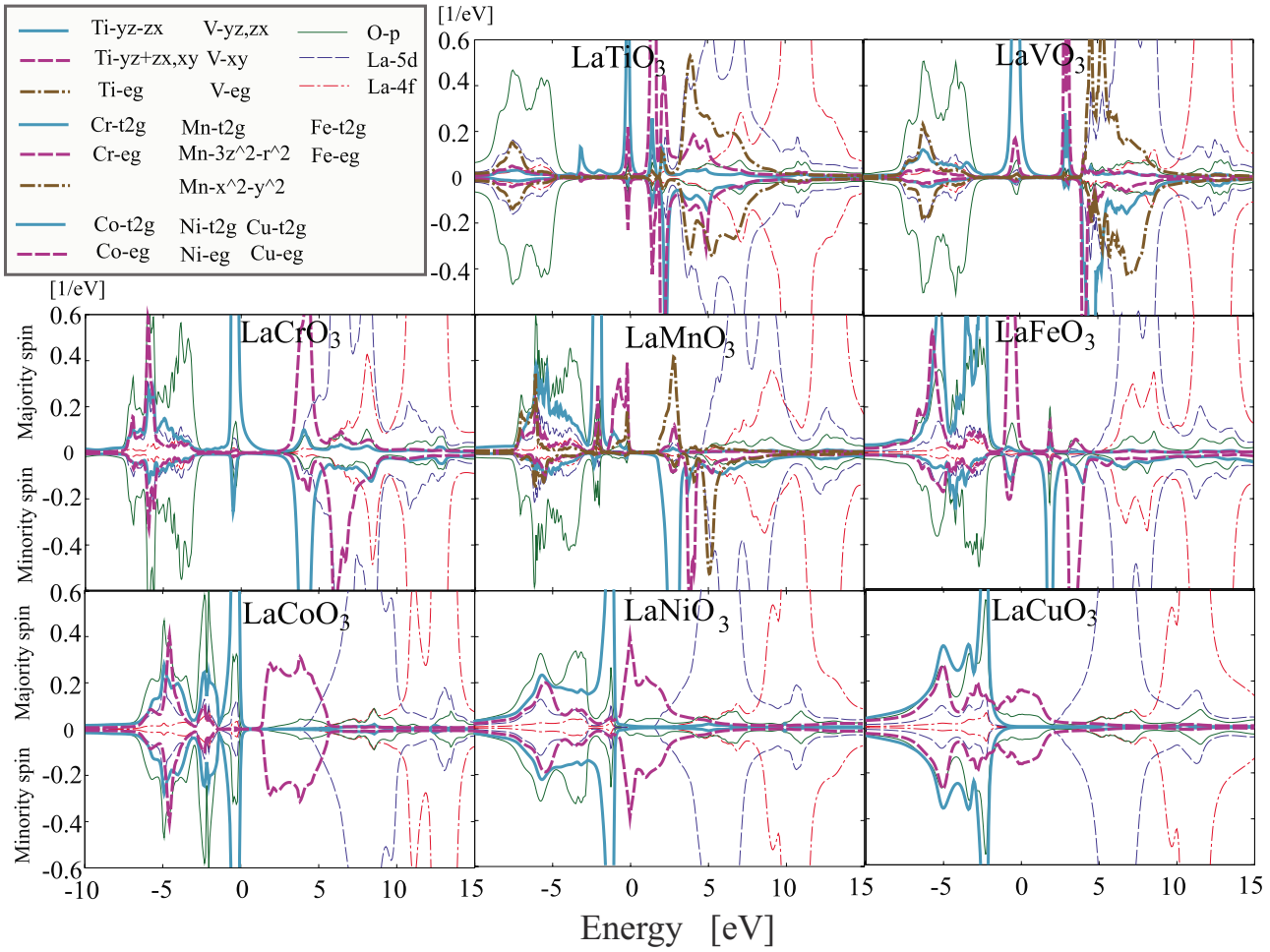


FIG. 5. (Color online) Imaginary part of the projected Green's functions per atom $(1/\pi)|\mathrm{Im}\, G(\omega)|$ of $LaMO_3$ ($M$=V~Cu) by U+GWA at third iteration. The energy zeroth is set at the Fermi energy $E_F$. The spectra of oxygen atom are the ones averaged over inequivalent sites. As for the transition-metal atoms, the spectra are those per atom of the spin-up site. The projected Im $G$ is depicted by using the local coordinate system where the $z$ axis is along the direction of $M$-O of the longest interatomic distance and other $x$ and $y$ axes direct to the other $M$-O. For all cases, La $4f$ orbitals are treated by U+GWA ($U$=7.5 eV, $J$=0.5 eV. Transition metal $U$ is used for Ti ($U$=2.5 eV, $J$=1.0 eV), V ($U$=3.0 eV, $J$=1.0 eV) and Co ($U$=2.7 eV, $J$=1.3 eV). Unit cells of $LaMO_3$ ($M$=Ti,V,Cr,Mn,Fe), contain four molecular units and those of $M$=Co, Ni and Cu contain one unit.

nents of $t_{2g}$ orbitals $d_{(yz+xz)/\sqrt{2}}$ and $d_{xy}$ are almost degenerate and form the bonding and antibonding states with oxygen $2p$ orbitals.

### 2. $LaVO_3$

$LaVO_3$ is an antiferromagnetic insulator but the LSDA calculation tells that it should be an antiferromagnetic metal. The $G$-type orbital order (OO) was suggested under the $C$-type antiferromagnetic spin order by LSDA+U.[23] LSDA+U and U+GWA calculations give an insulating ground state with the electron configuration of $V^{3+}$ $(t_{2g}^{\uparrow})^2$.

The calculated band gap is estimated to be 2.48 eV (the direct gap) and, on the other hand, the experimentally observed Hubbard and CT gaps are 1.1 and 4.0 eV, respectively.[45] This discrepancy may be due to our larger $U$ value in U+GWA calculation for keeping a band gap finite.

We find bonding V $d$-O $p$, nonbonding O $p$, and V $d$ states at −5.5, −3.0, −0.5 eV, respectively, and the peak positions of valence and conduction bands are in good agreement with the experimental spectrum.[49] The bands just below and above the band gap originate from split $t_{2g}$ levels of majority spin, and $d_{yz}$ and $d_{zx}$ are occupied and $d_{xy}$ unoccupied (Fig. 5). This is the $G$-type orbital order (OO) suggested in Ref. 23.

Both the top of the occupied band and the bottom of unoccupied band are $t_{2g}^{\uparrow}$. The bands are broadened in U+GWA, owing to the shift of the V and La $d$ states, La $f$ states, and hybridization between V $d$ and O $p$ states, as seen in the case of $LaTiO_3$. The energy separation between two principal peaks of occupied $t_{2g}yz,zx$ and unoccupied $t_{2g}xy$ bands in U+GWA (at about −0.3 and 3.2 eV) is about 3.5 eV, which may be estimated as

$$\{E_T[(t_{2g}^{\uparrow})^3] - E_T[(t_{2g}^{\uparrow})^2]\} - \{E_T[(t_{2g}^{\uparrow})^2] - E_T[(t_{2g}^{\uparrow})^1]\} = u'_{t_{2g}} - j_{t_{2g}} = U - 1.17J. \quad (8)$$

Once we replace $U$ in Eq. (8) by $W(0)$ and $J$ by the used one in U+GWA, our calculated result, $W(0)$=4.73 eV, is con-

sistent with the above energy separation 3.5 eV. This separation is the Hubbard gap as assigned in the experiment.[49]

### 3. $LaCrO_3$

$LaCrO_3$ is a $G$-type antiferromagnetic insulator with the band gap of 3.4 eV.[45] Calculations give rise to insulating state as seen in [Figs. 4(a) and 4(b)]. The electron configuration of $Cr^{3+}$ is $(t_{2g}^{\uparrow})^3$, and $t_{2g}^{\uparrow}$ bands are fully occupied (Fig. 5). The spectra of U+GWA agree well with observed ones both in occupied and unoccupied bands.[50] The top of the occupied band is $t_{2g}^{\uparrow}$ and the bottom of the unoccupied ones are shared by $e_g^{\uparrow}$ and $t_{2g}^{\downarrow}$ bands. In other words, the conduction-band electrons extend over sublattices of different spins.

The lower part of majority spin $t_{2g}^{\uparrow}$ bands is strongly mixed with O $p$ bands, but still the upper part of the occupied $t_{2g}^{\uparrow}$ bands are separated from the main bands of O $2p$ states. The highest occupied Cr $3d$ states mix strongly with O $2p$ states and the Hubbard and CT gaps are indiscernible.[45] The peak positions of the lower occupied bands are at −4 and −6 eV in good agreement with the observed spectrum.[50] The conduction-band spectrum in U+GWA has the peak structure also in good agreement with observed ones; observed majority spin $e_g$ and minority spin $t_{2g}$ bands locate at 4 eV, minority spin $e_g$ bands at 7 eV and La states at 9 eV in XAS. The value of the band gap is 3.3 eV which agrees well with the observed one of 3.4 eV.

The energy separation between two principal peaks of occupied $t_{2g}^{\uparrow}$ and unoccupied $e_g^{\uparrow}$ bands in U+GWA (at about −0.5 and 4 eV) is about 4.5 eV, which may be estimated as

$$\{E_T[(t_{2g}^{\uparrow})^3](e_g^{\uparrow})^1 - E_T[(t_{2g}^{\uparrow})^3]\} - \{E_T[(t_{2g}^{\uparrow})^3] - E_T[(t_{2g}^{\uparrow})^2]\} = 3(u'' - j'') - 2(u'_{t_{2g}} - j_{t_{2g}}) = U - 0.15J, \quad (9)$$

where $u''$ and $j''$ are the Coulomb and exchange integrals between $t_{2g}$ and $e_g$ orbitals (averaged over three orbitals of $t_{2g}$ and two of $e_g$ orbitals). (See Appendix C.) Once we replace $U$ in Eq. (9) by $W(0)$ (though $J$ is unknown but may be at most 1 eV), our calculated result, $W(0)=4.28$ eV, is consistent with the above energy separation of 4.5 eV.

### 4. $LaMnO_3$

The lattice of $LaMnO_3$ is distorted by the Jahn-Teller effect, which splits the degenerate $e_g$ levels, and the electron configuration of $Mn^{3+}$ ion is $(t_{2g}^{\uparrow})^3(e_g^{\uparrow})^1$. Then this system is insulator even if we use $U=0$ as seen in Fig. 4. The LSDA+U (with $U=0$) calculation of $LaMnO_3$ underestimates the band gap and overestimates $d$-bandwidth. We can see that the width of the majority Mn $d$ $t_{2g}$ band in the energy region between −2.3 and −0.1 eV in the LSDA+U results becomes narrower in U+GWA, and that of the majority Mn $d_{3z^2-r^2}$ band in the energy region between −1.0 and 0 eV in the LSDA results becomes broader.

The experimentally observed spectrum shows a majority spin $t_{2g}$ level at −2 eV, $e_g$ levels at 0 and 2 eV, a minority spin $e_g$ levels at 5 and 7 eV, $t_{2g}$ level at 6.5 eV, and La $5d$ band at 6–9 eV.[35] These observations agree with our calculated results. The only difference is the fact that $t_{2g}^{\downarrow}$ band is observed at 2.5 eV in contrast to calculated $e_g^{\uparrow}$ band at the same energy position. The overall feature in calculated U+GWA spectrum is in good agreement with observed result of XPS and XAS. The band gap 1.6 eV by U+GWA is consistent well with observed one of 1.1 eV.

The energy separation between two principal peaks of occupied $e_g^{\uparrow}$ and unoccupied $e_g^{\uparrow}$ bands (at −0.5 and 2.5 eV) is about 3.0 eV,[35] which can be estimated as

$$\{E_T[(t_{2g}^{\uparrow})^3(e_g^{\uparrow})^2] - E_T[(t_{2g}^{\uparrow})^3 e_g^{\uparrow}]\} - \{E_T[(t_{2g}^{\uparrow})^3 e_g^{\uparrow}] - E_T[(t_{2g}^{\uparrow})^3]\} = u'_{|rme_g} - j_{|rme_g} = U - 1.52J, \quad (10)$$

where $u'_{|rme_g}$ and $j'_{|rme_g}$ are the Coulomb and exchange integrals between $e_g u$ and $e_g v$ orbitals. (See Appendix C.) Once we replace $U$ in Eq. (10) by $W(0)$ (though $J$ is unknown), our calculated result, $W(0)=3.82$ eV, is consistent with the above energy separation of 3.0 eV.

With the local coordinate system of the $z$ direction being parallel to the longest Mn-O bond, the local orbital $d_{3z^2-r^2}$ of the majority spin may be occupied and $d_{x^2-y^2}$ of the majority spin empty (though not completely). The density matrix for the spin density of $e_g$ shell on one particular Mn atom is

$$n_{mm'}^{\uparrow} - n_{mm'}^{\downarrow} = \begin{pmatrix} 0.695 & 0.063 \\ 0.063 & 0.260 \end{pmatrix}. \quad (11)$$

With diagonalizing the density matrix, the spin density of the occupied $e_g^{\uparrow}$ consists of 0.70 occupation of almost pure $|3z^2-r^2\rangle$ and 0.26 occupation of $|x^2-y^2\rangle$. The orbital order (OO) is of the $C$ type in A-AFM $LaMnO_3$,[26] ferromagnetic interlayer OO and antiferromagnetic interlayer spin order. No essential change is introduced by a finite $U$ value, e.g., $U=7.0$ eV, in LSDA+U.[51] The projected spectra are shown in Fig. 5 There are several reports of experiments: $C$-type antiferromagnetic OO by the resonant x-ray scattering[26] and OO of the type of $\cos\frac{\theta}{2}|3x^2-r^2\rangle+\sin\frac{\theta}{2}|y^2-z^2\rangle$ of $\theta=92°$ by ESR[27] and $\theta=106°$ by neutron diffraction[28] experiments. Both the JT distortion and superexchange interaction may be crucial to explain these observed OO.[25] The Pump-and-probe study has been reported with respect to the excitation of the ground state $d_{3z^2-r^2}$ to the empty state $d_{x^2-y^2}$.[52]

### 5. $LaFeO_3$

Electron configuration of $Fe^{3+}$ ion is $(t_{2g}^{\uparrow})^3(e_g^{\uparrow})^2$ in $LaFeO_3$. The LSDA+U calculation of $LaFeO_3$ gives a vanishingly small band gap and the U+GWA widens it. The top of the occupied band is $e_g^{\uparrow}$ and the bottom of the unoccupied band is $t_{2g}^{\downarrow}$.

The valence-band spectra by U+GWA are in good agreement with the experimental XPS.[38] There are O $2p$ and Fe $3d$ bonding states, $t_{2g}$, and $e_g$ states at −5, −2.5, and −1 eV, respectively, in the experimental XPS, and these are also in good agreement with the peaks at −5.5, −3, −1 eV in U+GWA. We could get good agreement between the calculated conduction-band spectra and experimental XAS,[38] if we would shift the experimental one by 1–2 eV to the lower energy side. It must be noted that the experimental XAS spectrum[38] was aligned so that the band gap agrees with the optical gap of Ref. 45 and, therefore, there might be still

some ambiguity in experimental spectra. In the conduction-band spectrum in the XAS, we observe the majority-spin bands of $t_{2g}$ at 3 eV, $e_g$ at 4.5 eV, and La $5d$ at 8–9.5 eV, respectively, which are corresponding to peaks at 2, 3.5, and 7–8.5 eV in the spectrum of U+GWA.

The energy separation between two principal peaks of occupied $t_{2g}^{\uparrow}$ and unoccupied $t_{2g}^{\downarrow}$ bands (at −3.0 and 2.0 eV) in calculated spectra is about 5.0 eV.[35] Therefore, the energy separation can be estimated theoretically as

$$\begin{aligned}&\{E_T[(t_{2g}^{\uparrow})^3(e_g^{\uparrow})^2(t_{2g}^{\downarrow})^1] - E_T[(t_{2g}^{\uparrow})^3(e_g^{\uparrow})^2\} - \{E_T[(t_{2g}^{\uparrow})^3(e_g^{\uparrow})^2] \\ &\quad - E_T[(t_{2g}^{\uparrow})^2(e_g^{\uparrow})^2]\} \\ &= \{2u'_{t_{2g}} + u_{t_{2g}} + 2u''\} - [2(u_{t_{2g}'} - j_{t_{2g}}) + 2(u'' - j'')] \\ &= U + 4.34J \end{aligned} \tag{12}$$

Once we replace $U$ in Eq. (12) by $W(0)$ (though $J$ is unknown and at most 1 eV), our calculated result, $W(0)=3.03$ eV, is presumably not inconsistent with the above energy separation of 5.0 eV.

### 6. $LaCoO_3$

$LaCoO_3$ is a nonmagnetic insulator with the rhombohedral symmetry at low temperatures and has no lattice distortion. Then the $Co^{3+}$ ion is in the low-spin state of the electron configuration $t_{2g}^6$: $^1A_1$ and the electron configuration is $(t_{2g}^{\uparrow})^3(t_{2g}^{\downarrow})^3$. The system changes to the intermediate spin state ($t_{2g}^5e_g$: $^3T_1$) at around 90 K.[20] The intermediate spin state may develop an orbital order[53] which has been reported in the x-ray diffraction data.[54]

A value $U=0$ gives rise to a metallic nonmagnetic state and, then, we should introduce an on-site Coulomb interaction of $U=2.7$ eV in $Co^{3+}$. Then the band gap opens between $t_{2g}$ and upper $e_g$ states. The occupations of $e_g^{\uparrow}$ and $e_g^{\downarrow}$ are about 0.6, respectively. In the experimental assignment, there are Co $3d$ at 2 eV and La $5d$ at 7–9 eV,[39] which correspond to the U+GWA calculated positions of 3 and 8 eV. In the valence-band spectrum, there exists peaks at −1, −3, and −5.5 eV in the XPS,[39] which are in good agreement with the peaks in U+GWA spectrum.

There is no principal peak characterizing a multiplet in unoccupied spectra. Even though, let us choose two principal structures in occupied $t_{2g}$ and unoccupied $e_g$ bands at −0.8 and 2.0–5.0 eV. Then, the energy separation between these states is about 2.8–5.8 eV,[35] and the corresponding energy separation may be estimated as

$$\begin{aligned}&\{E_T[(t_{2g}^{\uparrow})^3(e_g^{\uparrow})^2(t_{2g}^{\downarrow})^1] - E_T[(t_{2g}^{\uparrow})^3(e_g^{\uparrow})^2\} \\ &\quad - \{E_T[(t_{2g}^{\uparrow})^3(e_g^{\uparrow})^2] - E_T[(t_{2g}^{\uparrow})^3(e_g^{\uparrow})^1]\} \\ &= \{3u'_{t_{2g}} + 2u''\} - [3(u'' - j'') + (u'_{e_g} - j_{e_g})] \\ &= U + 2.47J. \end{aligned} \tag{13}$$

Once we replace $U$ in Eq. (13) by $W(0)$ (though $J$ is unknown and at most 1 eV), our calculated result, $W(0)=4.73$ eV, is, at least, not inconsistent with the above energy separation of 2.0–5.0 eV.

### 7. $LaNiO_3$

$LaNiO_3$ is a paramagnetic metallic system with the rhombohedral symmetry and has no lattice distortion. Therefore, we expect that a value $U=0$ can lead to a good result. The band near the Fermi energy is $e_g$ which is separated from $t_{2g}$ bands.

The results of U+GWA are consistent with the experimental observation.[40] In the experimental spectrum of $LaNiO_3$, there are Ni $3d$ and La $5d$ at 0–2 and 6–8 eV, respectively, which are in good agreement with the peaks at 0–2 and 4.5–6.5 eV in U+GWA.

### 8. $LaCuO_3$

$LaCuO_3$ is a paramagnetic metallic system with the tetragonal symmetry and has no lattice distortion. Then, we expect that a value $U=0$ can lead to a good result as $LaNiO_3$. The band near the Fermi energy is $e_g$ which is separated from $t_{2g}$ bands. The results of U+GWA are consistent with the experimental observation,[41] the overall profile of the spectra and the positions of broad peaks. In the experimental spectrum of $LaCuO_3$, there are Cu $3d$ at 0–2 eV, La $5d$, $4f$, Cu $4s$, and $4p$ at 4–15 eV, which correspond to $3d$ at 0 eV, La $5d$ at 5–7 eV, La $4f$ at 11 eV. The $d$ orbitals of Cu are hybridized strongly with O $2p$ orbitals in the entire energy range.

## VI. SUMMARY

We studied the electronic structure of $LaMO_3$ ($M$=Ti ~ Cu) systematically by means of U+GWA at the first time with the careful treatment of the dynamical screening effects and the hybridization mixing between $M$ $3d$ and O $2p$ orbitals. We introduced finite values of $U$ into La $4f$ orbitals, so that La $5d$ orbitals do not hybridize with La $4f$. This procedure can keep correct energy levels of La $5d$ and $4f$ successfully in LSDA+U and U+GWA. We introduced the on-site Coulomb interaction $U$ also into the localized $d$ orbitals of $Ti^{3+}$, $V^{3+}$, and $Co^{3+}$. Other transition-metal ions $M^{3+}$ are affected by larger screening effects and they do not require finite $U$. The spectra obtained so far show an excellent agreement with the observed spectra and the resultant static-screened Coulomb interaction is consistent with the separation of principal peaks of the observed spectra. The legitimacy of U+GWA is made clear by analysis of mixing ratio of wave functions in Appendix B.

## ACKNOWLEDGMENTS

Our GWA program package, named GW-LMTO program package, will be soon available. Calculations were done at the Supercomputer Center, Institute for Solid State Physics, The University of Tokyo. This work was partially supported by a Grant-in-Aid for Scientific Research in Priority Areas "Development of New Quantum Simulators and Quantum Design" Grant No. 170640004 of The Ministry of Education, Culture, Sports, Science, and Technology in Japan.

## APPENDIX A: NUMERICAL TECHNIQUES: SAVING CPU-TIME AND DISK SPACE WITHOUT LOSS OF ACCURACY IN A SYSTEM WITH LARGE UNIT CELL

The perovskite-type transition-metal oxides have a large unit cell and, therefore, several kinds of new algorithms and programming techniques are essentially important for GWA calculation. We explain here various efforts for more accurate calculation and those for reducing the CPU time and saving the memory size without loss of accuracy.

### 1. Analytical approximant for self-energy

We calculate the imaginary part of the correlation part of the self-energy $\Sigma_C$ and, then, get its real part with the help of Kramers-Kronig transformation.[55] For this transformation, large number of the energy mesh points is necessary for an enough accuracy. Usually we divide the real energy axis into several hundreds mesh points and the resultant cost of the $\Sigma_C$ calculation becomes heavy. Then, a new method is essentially important to adopt smaller number of energy mesh points without loss of accuracy in order to reduce the CPU time.

First, we calculate the correlation part of screened Coulomb interaction $W_C$ at energy mesh points along the real energy axis, which is usually chosen with nonequal intervals. Then we represent $W_C$ as a sum of the first-order rational functions each of which has a single first-order pole at the midst point of each adjacent energy mesh points,

$$W^{\mathbf{kq}}_{C_{n'n}}(\omega) \equiv \langle \mathbf{k}-\mathbf{q}n:\mathbf{k}n' | W_C(\omega) | \mathbf{k}n':\mathbf{k}-\mathbf{q}n \rangle = \sum_j \left[ \frac{1}{\omega - z_j} - \frac{1}{\omega + z_j} \right] a^{\mathbf{kq}}_{n'nj}, \tag{A1}$$

where $z_j$ are points on the complex plane off from the real axis with an imaginary part of 1.5 times larger than the mesh point interval. The constant $a^{\mathbf{k}q}_{n'nj}$ is given as

$$a^{\mathbf{kq}}_{n'nj} = \sum_i [b^{-1}]_{ji} W^{\mathbf{kq}}_{C_{n'n}}(\omega_i), \tag{A2}$$

$$b_{ij} = \frac{1}{\omega_i - z_j} - \frac{1}{\omega_i + z_j}, \tag{A3}$$

where $\omega_i$ are the energy mesh points for the polarization function. In other words, we represent the branch cut as a dense set of the first-order poles. By using this analytical form of $W_C$, $\Sigma_C$ can be evaluated analytically. One example of $W^{\mathbf{kq}}_{C_{n'n}}(\omega)$ is shown in Fig. 6.

We can control and reduce the number of energy mesh points and this fitting method can actually reduce the CPU time, without loss of numerical accuracy, for the calculation of the polarization $P$ and $\Sigma_C$ by factors $\frac{1}{4}$ and $\frac{1}{2}$, respectively. Moreover, also the disk space and the memory size for the calculation of the polarization can become smaller by a factor $\frac{1}{4}$.

### 2. Parallelization

The calculations of large systems, such as the cubic perovskite with the tilt and distortion of $MO_6$ octahedron, requires much CPU time. Parallelization algorithm in calculation of polarization and self-energy is desirable.

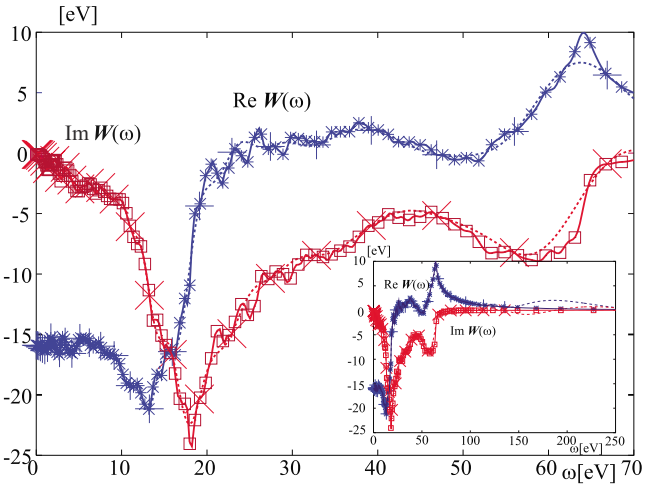


FIG. 6. (Color online) Real and imaginary parts of $W^{\mathbf{kq}}_{C_{n'n}}(\omega)$ of $LaMnO_3$, where $n=n'=$valence band bottom, $\mathbf{k}=(0,0,0)$ and $\mathbf{q}=\frac{\pi}{c}(0,0,\frac{1}{2})$, where $c$ is the lattice constant along the $c$ axis. Marks represent the calculated points, 128 points and 32 points data, and the solid and dotted lines are the results fitted by the rational function Eq. (A1).

In the previous work,[5] we parallelized only the $\omega$ loop by Open MP with 64 CPUs in the calculation of $P$ and $\Sigma_C$. In the present work, we use 64 CPUs with 4 parallel $\mathbf{q}$ loops and 16 parallel $\omega$ loops. This procedure results in higher efficiency. We notice that the conversion matrix from $\psi^*_{k'}\psi_{k'+q}$ to the product basis requires a large memory size and we divide the loop to allocate the memory of this matrix with reduction of memory size more efficiently.

### 3. Crystal symmetry

The correlation part of the self-energy $\Sigma_C$ is expressed as

$$\Sigma_C(\mathbf{k},\epsilon) = i\sum_{\mathbf{q}} w_{\mathbf{q}} \int \frac{d\omega}{2\pi} G_0(\mathbf{k}-\mathbf{q},\epsilon-\omega) W_C(\mathbf{q},\omega), \tag{A4}$$

where $w_{\mathbf{q}}$ is the weight of $\mathbf{q}$ point and $G_0$ is the unperturbed Green's function. The polarization $P(\mathbf{q},\omega)$ is necessary to calculate $W_C$. The CPU time and memory size become huge for both $P$ and $\Sigma_C$. In the previous work,[5] we calculated $P$ for all $\mathbf{q}$ points. In the present work, the symmetry operations in crystals are implemented and we calculate the polarization $P$ only at inequivalent $\mathbf{q}$ points in the irreducible zone. The calculation of the polarization becomes faster and needs much smaller disk space.

## APPENDIX B: OFF-DIAGONAL ELEMENTS OF SELF-ENERGY

In order to see how good initial wave functions we make for GWA, we evaluate the mixing amplitude of those wave functions by the off-diagonal element of the self-energy.[4]

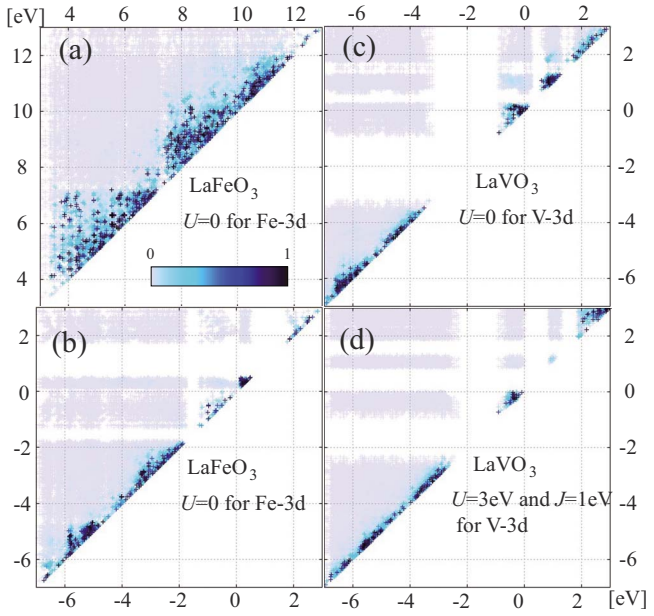


FIG. 7. (Color online) The mixing ratios of wave functions $(\sqrt{x^2+1}-x)^2$ are shown for $LaFeO_3$ and $LaVO_3$ with the parameters of $U=7.5$ eV and $J=0.5$ eV for La $4f$. (a) La $4f$ and $5d$ region (3 eV$<E<$13 eV) in $LaFeO_3$ where $U=0$ and $J=0$ for Fe, (b) near Fermi level $E_F$ (−7 eV$<E<$3 eV) in $LaFeO_3$ where $U=0$ and $J=0$ for Fe, (c) $U=0$ and $J=0$ for V $3d$ in $LaVO_3$, (d) $U=3.0$ eV and $J=1.0$ eV for V $3d$ in $LaVO_3$. The vertical and horizontal axis are the LSDA+U eigenenergies $\epsilon_{\mathbf{k}n}$ and $\epsilon_{\mathbf{k}n'}$ for U+GWA and the energy zeroth is set to the Fermi energy of LSDA+U calculation.

When the off-diagonal matrix element of the self-energy $\Delta\Sigma_{\mathbf{k}nn'}$ is finite, two bands $n$ and $n'$ at $\mathbf{k}$ (LSDA+U eigenenergies $\epsilon_{\mathbf{k}n}$ and $\epsilon_{\mathbf{k}n'}$) may be mixed. The effective Hamiltonian matrix is the $2\times2$ matrix;

$$\begin{pmatrix} \epsilon_{\mathbf{k}n}+\Delta\Sigma_{\mathbf{k}n}(\epsilon_{\mathbf{k}n}) & \Delta\Sigma_{\mathbf{k}nn'}(\{\epsilon_{\mathbf{k}n}+\epsilon_{\mathbf{k}n'}\}/2) \\ \Delta\Sigma^{*}_{\mathbf{k}nn'}(\{\epsilon_{\mathbf{k}n}+\epsilon_{\mathbf{k}n'}\}/2) & \epsilon_{\mathbf{k}n'}+\Delta\Sigma_{\mathbf{k}n'}(\epsilon_{\mathbf{k}n'}) \end{pmatrix}. \tag{B1}$$

By diagonalizing this matrix, we evaluate the mixing ratio as

$$(\sqrt{x^2+1}-x)^2{:}1, \tag{B2}$$

where

$$x=\left|\frac{\epsilon_{\mathbf{k}n}+\Delta\Sigma_{\mathbf{k}n}(\epsilon_{\mathbf{k}n})-\epsilon_{\mathbf{k}n'}-\Delta\Sigma_{\mathbf{k}n'}(\epsilon_{\mathbf{k}n'})}{2\Delta\Sigma_{\mathbf{k}nn'}(\{\epsilon_{\mathbf{k}n}+\epsilon_{\mathbf{k}n'}\}/2)}\right|. \tag{B3}$$

When this ratio is small ($x$ is much larger than the unity), the resultant mixing is negligible. We will justify the approximation by using these formula.

In fact, a finite $U$ value improves starting wave functions by changing their locality and the legitimacy may be approved by calculating the off-diagonal elements of the resultant self-energy. Figure 7 shows the mixing ratios in $LaFeO_3$ ($U=0$ eV) and $LaVO_3$ ($U=0$ and 3.0 eV) per spin for the elements between $\{\mathbf{k}n\}$ and $\{\mathbf{k}n'\}$.

Figure 7(a) shows the mixing ratio in the energy range of La $4f$ and $5d$ bands in $LaFeO_3$, which indicates that there is no hybridization (appreciable matrix elements) between La $4f$ and $5d$ states. This is the direct result of our introduction of $U$ in La $4f$. On the contrary, calculation without $U$ of La $4f$ causes strong hybridization between La $4f$ and $5d$ bands and GWA could not split them.

In the energy region near $E_F$ in $LaFeO_3$, no elements have larger mixing ratio in Fig. 7(b). It is not needed to start with LSDA+U method for Fe $3d$ orbitals. In other words, $LaFeO_3$ has large screening effects and resultantly the screened on-site Coulomb interaction becomes small.

One should compare Figs. 7(c) and 7(d) for the results of $U=0$ and 3.0 eV in V $3d$ orbitals. One may notice that the area of larger mixing ratio appears near $E_F$ in GWA of $U=0$ eV [Fig. 7(c)], because the system is metallic in LSDA. On the contrary, in the case of $U=3.0$ eV [Fig. 7(d)], the LSDA+U method improves the starting wave functions and no large off-diagonal elements of the self-energy are seen in U+GWA. Resultant system becomes insulator by U+GWA and the energy gap opens. This indicates that GWA could not improve the problem of small screening effects in $LaVO_3$ and requires LSDA+U wave functions.

## APPENDIX C: COULOMB INTERACTIONS

The effective Coulomb and exchange integrals between orbitals $\phi_a$ and $\phi_b$, $U(a,b)$ and $J(a,b)$, are represented by the Racah parameters $A$, $B$, and $C$ or by the Slater integrals $F_0$, $F_2$, and $F_4$. The Coulomb and exchange interactions[4] of $d$ orbitals are as follows in the cubic symmetry,

$$u_{t_{2g}}=U(\xi,\xi)=U(\eta,\eta)=U(\zeta,\zeta)=u_{e_g}=U(u,u)=U(v,v)=A+4B+3C=F_0+4F_2+36F_4, \tag{C1}$$

$$u'_{t_{2g}}=U(\xi,\eta)=U(\eta,\zeta)=U(\zeta,\xi)=A-2B+C=F_0-2F_2-4F_4, \tag{C2}$$

$$u'_{e_g}=U(u,v)=A-4B+C=F_0-4F_2+6F_4, \tag{C3}$$

$$u''=\frac{1}{6}\sum_{a\in t_{2g}}\sum_{b\in e_g}U(a,b)=A+C=F_0-14F_4, \tag{C4}$$

$$j_{t_{2g}}=J(\xi,\eta)=J(\eta,\zeta)=J(\zeta,\xi)=3B+C=3F_2+20F_4, \tag{C5}$$

$$j_{e_g}=J(u,v)=4B+C=4F_2+15F_4, \tag{C6}$$

$$j''=\frac{1}{6}\sum_{a\in t_{2g}}\sum_{b\in e_g}J(a,b)=2B+C=2F_2+25F_4, \tag{C7}$$

We have an empirical relationship[1] $F_4/F_2=0.63/9=0.07$ and the above expressions are rewritten in terms of the Coulomb and exchange parameters $U$ and $J$ as

$$u_{t_{2g}}=u_{e_g}=U+1.14J, \tag{C8}$$

$$u'_{t_{2g}} = U - 0.40J, \tag{C9}$$

$$u'_{e_g} = U - 0.63J, \tag{C10}$$

$$j_{t_{2g}} = 0.77J, \tag{C11}$$

$$j_{e_g} = 0.89J, \tag{C12}$$

$$u'' = U - 0.17J, \tag{C13}$$

$$j'' = 0.66J, \tag{C14}$$

where $U=F_0$ and $J=\frac{7}{2}(F_2+9F_4)$. These $U$ and $J$ are the parameters of LSDA+U or correspond to the output Coulomb and exchange interactions in U+GWA.


[1] A. I. Liechtenstein, V. I. Anisimov, and J. Zaanen, Phys. Rev. B **52**, R5467 (1995). The definition of $U$ and $J$ is given in this paper.

[2] L. Hedin, Phys. Rev. **139**, A796 (1965).

[3] M. S. Hybertsen and S. G. Louie, Phys. Rev. B **34**, 5390 (1986).

[4] S. Kobayashi, Y. Nohara, S. Yamamoto, and T. Fujiwara, Phys. Rev. B **78**, 155112 (2008).

[5] Y. Nohara, A. Yamasaki, S. Kobayashi, and T. Fujiwara, Phys. Rev. B **74**, 064417 (2006).

[6] M. P. Surh, S. G. Louie, and M. L. Cohen, Phys. Rev. B **43**, 9126 (1991).

[7] M. Springer, F. Aryasetiawan, and K. Karlsson, Phys. Rev. Lett. **80**, 2389 (1998).

[8] V. I. Anisimov, F. Aryasetiawan, and A. I. Lichtenstein, J. Phys.: Condens. Matter **9**, 767 (1997).

[9] O. K. Andersen and O. Jepsen, Phys. Rev. Lett. **53**, 2571 (1984); O. K. Andersen, O. Jepsen, and D. Glötzel, in *Canonical Description of the Band Structures of Metals*, Proceedings of the International School of Physics, "Enrico Fermi," Course LXXXIX, Varenna, 1985, edited by F. Bassani, F. Fumi, and M. P. Tosi, (North-Holland, Amsterdam, 1985), p. 59.

[10] F. Aryasetiawan and O. Gunnarsson, Phys. Rev. B **49**, 16214 (1994).

[11] A. Yamasaki and T. Fujiwara, Phys. Rev. B **66**, 245108 (2002).

[12] A. Yamasaki and T. Fujiwara, J. Phys. Soc. Jpn. **72**, 607 (2003).

[13] V. I. Anisimov and O. Gunnarsson, Phys. Rev. B **43**, 7570 (1991).

[14] E. O. Wollan and W. C. Koehler, Phys. Rev. **100**, 545 (1955).

[15] J. P. Goral and J. E. Greedan, J. Magn. Magn. Mater. **37**, 315 (1983).

[16] V. G. Zubkov, G. V. Bazuev, V. A. Parelyaev, and G. P. Shveikin, Sov. Phys. Solid State **15**, 1079 (1973).

[17] P. Dougier and P. Hagenmuller, J. Solid State Chem. **11**, 177 (1974).

[18] W. C. Koehler and E. O. Wollan, J. Phys. Chem. Solids **2**, 100 (1957).

[19] F. Moussa, M. Hennion, J. Rodriguez-Carvajal, H. Moudden, L. Pinsard, and A. Revcolevschi, Phys. Rev. B **54**, 15149 (1996).

[20] T. Saitoh, T. Mizokawa, A. Fujimori, M. Abbate, Y. Takeda, and M. Takano, Phys. Rev. B **55**, 4257 (1997).

[21] K. Sreedhar, J. M. Honig, M. Darwin, M. McElfresh, P. M. Shand, J. Xu, B. C. Crooker, and J. Spalek, Phys. Rev. B **46**, 6382 (1992).

[22] M. Cwik, T. Lorenz, J. Baier, R. Muller, G. Andre, F. Bouree, F. Lichtenberg, A. Freimuth, R. Schmitz, E. Muller-Hartmann, and M. Braden, Phys. Rev. B **68**, 060401(R) (2003).

[23] H. Sawada, N. Hamada, K. Terakura, and T. Asada, Phys. Rev. B **53**, 12742 (1996).

[24] J. B. Goodenough, Phys. Rev. **100**, 564 (1955); J. Kanamori, J. Phys. Chem. Solids **10**, 87 (1959).

[25] S. Okamoto, S. Ishihara, and S. Maekawa, Phys. Rev. B **65**, 144403 (2002).

[26] Y. Murakami, J. P. Hill, D. Gibbs, M. Blume, I. Koyama, M. Tanaka, H. Kawata, T. Arima, Y. Tokura, K. Hirota, and Y. Endoh, Phys. Rev. Lett. **81**, 582 (1998).

[27] J. Deisenhofer, B. I. Kochelaev, E. Shilova, A. M. Balbashov, A. Loidl, and H. A. Krug von Nidda, Phys. Rev. B **68**, 214427 (2003).

[28] J. Rodriguez-Carvajal, M. Hennion, F. Moussa, A. H. Moudden, L. Pinsard and A. Revcolevschi, Phys. Rev. B **57**, R3189 (1998).

[29] P. Bordet, C. Chaillout, M. Marezio, Q. Huang, A. Santoro, S.-W. Cheong, H. Takagi, C. S. Oglesby, and B. Batlogg, J. Solid State Chem. **106**, 253 (1993).

[30] C. P. Khattak and D. E. Cox, Mater. Res. Bull. **12**, 463 (1977).

[31] S. E. Dann, D. B. Currie, M. T. Weller, M. F. Thomas, and A. D. Al-Rawwas, J. Solid State Chem. **109**, 134 (1994).

[32] J. F. Bringley, B. A. Scott, S. J. La Placa, T. R. McGuire, F. Mehran, M. W. McElfresh, and D. E. Cox, Phys. Rev. B **47**, 15269 (1993).

[33] N. N. Kovaleva, A. V. Boris, C. Bernhard, A. Kulakov, A. Pimenov, A. M. Balbashov, G. Khaliullin, and B. Keimer, Phys. Rev. Lett. **93**, 147204 (2004).

[34] T. Saitoh, A. E. Bocquet, T. Mizokawa, and A. Fujimori, Phys. Rev. B **52**, 7934 (1995).

[35] T. Saitoh, A. E. Bocquet, T. Mizokawa, H. Namatame, A. Fujimori, M. Abbate, Y. Takeda, and M. Takano, Phys. Rev. B **51**, 13942 (1995).

[36] A. E. Bocquet, T. Mizokawa, K. Morikawa, A. Fujimori, S. R. Barman, K. Maiti, D. D. Sarma, Y. Tokura, and M. Onoda, Phys. Rev. B **53**, 1161 (1996).

[37] A. E. Bocquet, T. Mizokawa, T. Saitoh, H. Namatame, and A. Fujimori, Phys. Rev. B **46**, 3771 (1992).

[38] H. Wadati, D. Kobayashi, H. Kumigashira, K. Okazaki, T. Mizokawa, A. Fujimori, K. Horiba, M. Oshima, N. Hamada, M. Lippmaa, M. Kawasaki, and H. Koinuma, Phys. Rev. B **71**, 035108 (2005).

[39] M. Abbate, J. C. Fuggle, A. Fujimori, L. H. Tjeng, C. T. Chen, R. Potze, G. A. Sawatzky, H. Eisaki, and S. Uchida, Phys. Rev. B

**47**, 16124 (1993).
[40] M. Abbate, G. Zampieri, F. Prado, A. Caneiro, J. M. Gonzalez-Calbet, and M. Vallet-Regi, Phys. Rev. B **65**, 155101 (2002).
[41] T. Mizokawa, A. Fujimori, H. Namatame, Y. Takeda, and M. Takano, Phys. Rev. B **57**, 9550 (1998).
[42] F. M. F. de Groot, J. C. Fuggle, B. T. Thole, and G. A. Sawatzky, Phys. Rev. B **42**, 5459 (1990).
[43] E. F. Bertaut, J. Mareschal, G. De Vries, R. Aleonard, R. Pauthenet, J. P. Rebouillat, and V. Zarubicka, IEEE Trans. Magn. **2**, 453 (1966).
[44] X.-D. Zhou, L. R. Pederson, Q. Cai, J. Yang, B. J. Scarfino, M. Kim, W. B. Yelon, W. J. James, H. U. Anderson, and C. Wang, J. Appl. Phys. **99**, 08M918 (2006).
[45] T. Arima, Y. Tokura, and J. B. Torrance, Phys. Rev. B **48**, 17006 (1993).
[46] F. Aryasetiawan, M. Imada, A. Georges, G. Kotliar, S. Biermann, and A. I. Lichtenstein, Phys. Rev. B **70**, 195104 (2004).
[47] One may expect that the band gap would become narrower by 0.1–0.2 eV as observed in Im $G$ in the ferromagnetic Fe and Ni.
V. P. Zhukov, E. V. Chulkov, and P. M. Echenique, Phys. Rev. Lett. **93**, 096401 (2004).
[48] M. Nakamura, T. Yoshida, K. Mamiya, A. Fujimori, Y. Taguchi, and Y. Tokura, Mater. Sci. Eng., B **68**, 123 (1999).
[49] K. Maiti and D. D. Sarma, Phys. Rev. B **61**, 2525 (2000).
[50] D. D. Sarma, N. Shanthi, and P. Mahadevan, Phys. Rev. B **54**, 1622 (1996).
[51] J. E. Medvedeva, M. A. Korotin, V. I. Anisimov, and A. J. Freeman, Phys. Rev. B **65**, 172413 (2002).
[52] H. Tamaru, K. Ishida, N. Ogawa, Y. Kubo, and K. Miyano, Phys. Rev. B **78**, 075119 (2008).
[53] M. A. Korotin, S. Yu. Ezhov, I. V. Solovyev, V. I. Anisimov, D. I. Khomskii, and G. A. Sawatzky, Phys. Rev. B **54**, 5309 (1996).
[54] G. Maris, Y. Ren, V. Volotchaev, C. Zobel, T. Lorenz, and T. T. M. Palstra, Phys. Rev. B **67**, 224423 (2003).
[55] F. Aryasetiawan and O. Gunnarsson, Rep. Prog. Phys. **61**, 237 (1998).